Supporting Information

Nitrogen Reduction through Confined Electro-catalysis with Carbon Nanotube Inserted Metal Organic Frameworks

Yang Lv[a], Yiqi Wang[a], Miao Yang[a], Zhangyan Mu[a], Shengtang Liu[a], Weiping Ding[a], Mengning Ding[*a]

[a] Key Lab of Mesoscopic Chemistry, School of Chemistry and Chemical engineering, Nanjing University, Nanjing 210023, China. Email: mding@nju.edu.cn

1. Supplementary experimental procedure

1.1. Chemical

All reagents were commercially obtained without further treatment. Zircomiun tetrachloride ($ZrCl_4$), bismuth nitrate pentahydrate ($Bi(NO_3)_3 \cdot 5H_2O$), Iron (III) nitrate nonahydrate ($Fe(NO_3)_3 \cdot 9H_2O$), 1,4-benzenedicarboxylic acid (H_2BDC), multi-walled carbon nanotubes (CNTs), N-doped multi-walled carbon nanotubes (NCNTs), sodium nitroferricyanide and p-dimethylaminobenzaldehyde were obtained from the Shanghai Macklin Biochemical Co., Ltd. Cerium (III) nitrate hexahydrate ($Ce(CO_3)_3 \cdot 6H_2O$), salicylic acid, 1,3,5-benzenetricarboxylic acid (H_3BTC), sodium hydroxide (NaOH) and sodium dihydrogen citrate were obtained from the Adamas Reagent Co., Ltd. Ethanol (EtOH), methanol (MeOH), acetone, sulfuric acid (H_2SO_4), hydrochloric acid (HCl), Hydrazine dihydrochlorideand ($N_2H_4 \cdot 2HCl$), N,N-dimethylformamide (DMF) were obtained from the Sinopharm Chemical Reagent Co., Ltd. Sodium hypochlorite (NaClO, 11-14% available chlorine) and 5 wt% Nafion solution were obtained from the Alfa Aesar. 1,3,5-tris(4-carboxyphenyl)benzene (BTB) was obtained from the Boka-chem Co., Ltd. DI water (18.2 MΩ·cm at 25°C, TOC<5ppb) used in this study was

obtained from Milli-Q Intergral 3 System (Merck Millipore).

1.2. Synthesis of UIO-66 system

The UIO-66 was prepared following a previously reported method (UIO-66).[1] In detail, the UIO-66 precursor was prepared by dissolving $ZrCl_4$ (0.536 g) and H_2BDC (0.5 g) in 60 mL DMF at room temperature. The obtained mixture was sealed in a Teflon-reactor and held at 120 °C for 24 h. After cooling to room temperature, the resulted white solid was collected by centrifugation, washed with DMF and MeOH each for 3 times, and was dried under 70 °C overnight. The final product was identified by XRD as UIO-66. In addition, CNT@UIO-66 and NCNT@UIO-66 were synthesized following the same procedure, in the presence of CNT (20 mg) and NCNT (20 mg).

1.3. Synthesis of BIT-58 system

The BIT-58 was prepared following a previously reported method (BIT-58).[2] In detail, the BIT-58 precursor was prepared by dissolving $Ce(NO_3)_3 \cdot 6H_2O$ (0.5544 g) and BTB (0.192 g) in 65 mL DMF/MeOH/H_2O (6 : 6 : 1) mixed solution with ultrasound for about 30 min at room temperature The obtained mixture was sealed in a Teflon-reactor and held at 85 °C for 24 h. After cooling to room temperature, the resulted light yellow bulk crystals were collected by centrifugation, washed with DMF and MeOH each for 3 times, and were dried under 70 °C overnight. The final product was indentified by XRD as BIT-58. In addition, CNT@BIT-58 and NCNT@BIT-58 were synthesized following the same procedure, in the presence of CNT (20 mg) and NCNT (20 mg).

1.4. Synthesis of CAU-17 system

The CAU-17 was prepared following a previously reported method (CAU-17).[3] In detail, the CAU-17 precursor was prepared by dissolving ground $Bi(NO_3)_3 \cdot 5H_2O$ (0.15 g) and H_3BTC (0.75 g) in 60 mL MeOH at room temperature. The obtained mixture was sealed in a Teflon-reactor and held at 120 °C for 24 h. After cooling to room temperature, the resulted white powder was collected by centrifugation, washed with MeOH for 5 times and acetone for one

time, and was dried under 70 $^{\circ}$C overnight. The final product was identified by XRD as CAU-17. In addition, CNT@CAU-17 and NCNT@CAU-17 were synthesized following the same procedure, in the presence of CNT (20 mg) and NCNT (20 mg).

1.5. Synthesis of MIL-101(Fe) system

The MIL-101(Fe) was prepared following a previously reported method (MIL-101(Fe)).[4] In detail, the MIL-101(Fe) precursor was prepared by dissolving $Fe(NO_3)_3 \cdot 9H_2O$ (2.4 g) and H_2BDC (0.984 g) in 60 mL DMF at room temperature. The obtained mixture was sealed in a Teflon-reactor and held at 150 $^{\circ}$C for 16 h. After cooling to room temperature, the resulted brownish red products were collected by centrifugation, washed with DMF and MeOH each for 3 times, and was dried under 90 $^{\circ}$C overnight. The final product was identified by XRD as MIL-101(Fe). In addition, CNT@MIL-101(Fe) and NCNT@MIL-101(Fe) were synthesized following the same procedure, in the presence of CNT (20 mg) and NCNT (20 mg).

1.6. Preparation of the catalytic working electrodes

5 mg of the as-prepared catalyst was dispersed in mixed solution of deionized water (240 μL) and EtOH (720 μL), to give a homogeneous suspension after sonication for 30 min. Subsequently, 40 μL Nafion (5wt% in EtOH) was added and the suspension was sonicated for another 30 min. Then, 50 μL catalyst ink was dropped on a carbon paper electrode with an area of 1 cm^{-2} and dried at room temperature for 2 h. The mass loading of catalyst was *ca.* 0.25 mg cm^{-2}.

1.7. Electrochemical nitrogen reduction reaction (eNRR) measurements

Electrochemical measurements were carried out with an H-type cell (15 mL in volume) separated by a Nafion 211 membrane at room temperature and atmospheric pressure, with a potentiostat CHI 750E. In the NRR stability test, each catalyst was tested for six times. Before NRR tests, the membrane was pretreated in refer to the literature[1]. In specific, the membrane was protonated by first boiling in ultrapure water for 1 h and treating in H_2O_2 (5%) aqueous

solution at 80 °C for another 1 h, respectively. And then, the membrane was treated in 0.5 M H$_2$SO$_4$ for 3 h at 80 °C and finally in water for 6 h. Graphite rod and Ag/AgCl electrode were used as counter electrode and reference electrode, respectively. The electrolyte was 0.05 M H$_2$SO$_4$ and the total volume was 15 mL. The electrolyte was pre-saturated with N$_2$ or Ar gas bubbling for 1 h prior to each electrochemical measurement and continuously bubbled with corresponding gas at a flow rate of 15 sccm during the tests. The scan rate of the linear sweep voltammetry was set at a rate of 1 mV s^{-1} and the current densities were normalized by geometric surface areas. The NRR activity of a sample was evaluated using potentiostatic method for 2 h at room temperature. Readings for the Ag/AgCl electrode were converted to the reversible hydrogen electrode (RHE) according to the following relationship.

$$E(RHE) = E(Ag/AgCl) + 0.197V + 0.0592 \times pH$$

1.8. Ammonia quantification by indophenol blue method[5]

The concentration-absorbance curves were calibrated using standard NH$_3$ solution with varying concentrations (Fig. S8). The fifitting curve (y = 0.37467 x + 0.03152, R^2 = 0.999) shows good linear relation of absorbance value with NH$_3$ concentration. In detail, NH^{4+} standard solutions with specific concentrations were formed by dissolving a specific amount of (NH$_4$)$_2$SO$_4$ in 0.05 M H$_2$SO$_4$ aqueous solution to give 0~2.0 μg mL^{-1} concentration of NH^{4+}. Then, salicylic acid developer, sodium hypochlorite, and nitropurna were subsequently added into the standard solutions (with a ratio of 2 mL : 1 mL : 0.2 mL : 2 mL). After standing at room temperature for 2 hr, the UV-Vis absorption spectrum was measured at a wavelength of 655 nm to give a standard calibration curve. The quantity of the produced NH$_3$ from eNRR was determined as following: for the indophenol blue method, 2 mL of the post-electrolysis electrolyte was pipetted and mixed with 2 mL of NaOH solution (1 M) containing 5 wt% salicylic acid and 5 wt% sodium citrate. Then, 1 mL NaClO solution (0.05 M) and 200 μL sodium nitroferricyanide solution (1 wt%) were added into the mixture sequentially. After 2

hr, the mixed solution was tested by UV-vis spectrophotometer (UV-2600, Shimadzu) to obtain the absorption spectra, the peak value of which was then used with above calibration curve for the quantification of NH_3 production. The peak of the resulting indophenol blue was at *ca.* $\lambda = 655$ nm.

1.9. Hydrazine quantification by spectrophotometric method[6]

Absolute calibration of hydrazine was achieved using N_2H_4 solutions of known concentration as standards, and the fifitting curve shows good linear relation of absorbance with N_2H_4 concentration in 0.05 M H_2SO_4 (Fig. S9, y = 1.2004 x + 0.052, R^2 = 0.999). In detail, first, preparing a series of standard solutions (0~2.5 µg mL^{-1}); second, adding 5 mL prepared color reagent and staining for 2 h at room temperature; finally, the absorbance of the resulting solution was measured at 455 nm, and the yields of N_2H_4 were estimated from a standard curve using 5 mL residual electrolyte and 5 mL color reagent. The quantification of the hydrazine was determined by the spectrophotometric method. Briefly, 5 mL electrolyte was added into 5mL coloring solution which contained 4 g p-dimethylaminobenzaldehyde, 20 mL concentrated hydrochloric acid and 200 mL ethanol. After 15 min, the absorbance at *ca.* $\lambda = 455$ nm of the resulting solution was collected by using UV-vis spectrophotometer (Shimadzu UV-2600).

1.10. Calculation of the NH_3 yield rate and faradaic efficiency

The NH_3 yield rate was calculated as follows:

$$NH_3 \text{ } yield \text{ } rate = \frac{C_{NH_3} \times V}{t \times mg_{cat}}$$

The faradaic efficiency was estimated from the charge consumed for NH_3 production and the total transfer during NRR test:

$$Faradaic\ Efficiency = \frac{3 \times C_{NH_3} \times V \times F}{17Q}$$

where C_{NH_3} is the concentration of the measured ammonia, V is the volume of the electrolyte, t is the reduction time, mg_{cat} is the amount of the catalyst on the electrode, F is the Faraday constant (96485 C mol^{-1}) and Q is the total transferred charge during NRR test.

1.11. Isotope-labelled experiments

The electrolyte was firstly bubbled with Ar for 1 h, and then electrolyzed with $^{15}N_2$ (99 at%) at -0.45 V vs. RHE in 0.05 M H_2SO_4, the obtained $^{15}NH^{4+}$ was qualitatively determined by ^1H nuclear magnetic resonance. In detail, 15 mL of the electrolyte was taken out and concentrated to 1 mL by heating at 80 °C. Afterwards, 0.9 mL of the above electrolyte was taken out and mixed with 0.1 mL DMSO-d_6 as an internal standard for ^1H NMR measurement.

2. Supplementary figures and tables
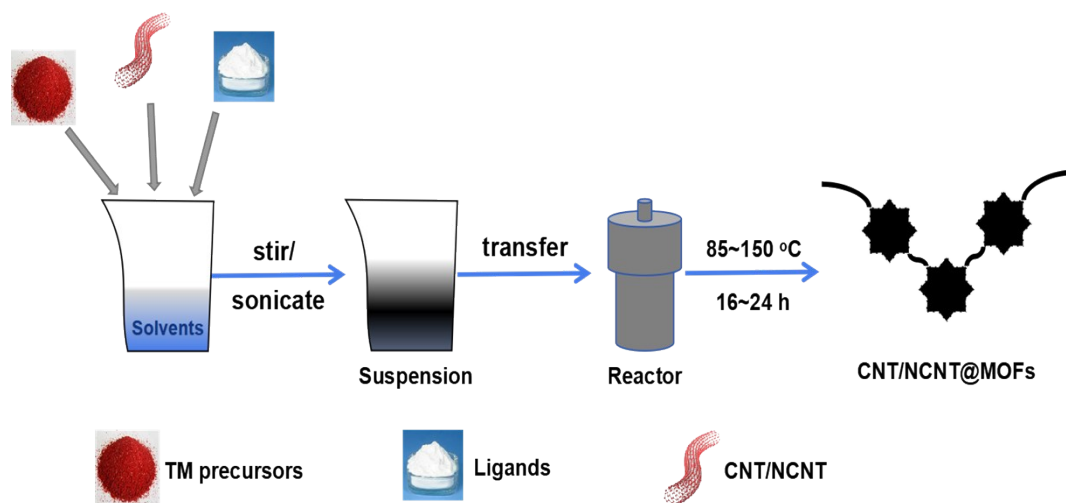
Fig. S1. Scheme of the synthesis of CNT/NCNT@MOFs.
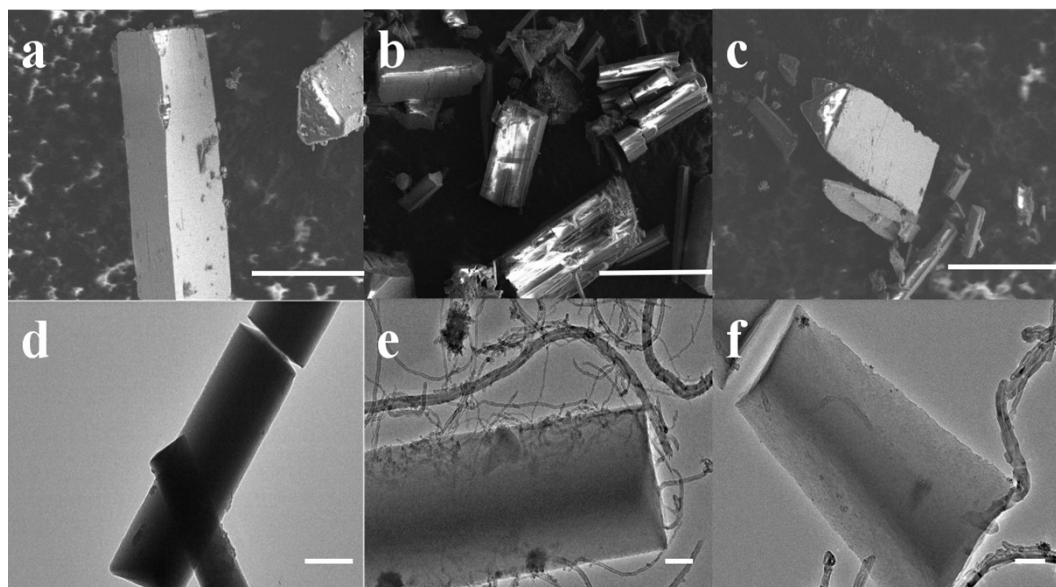
Fig. S2. SEM images of (a) BIT-58, (b) CNT@BIT-58, and (c) NCNT@BIT-58. TEM images of (d) BIT-58, (e) CNT@BIT-58, and (f) NCNT@BIT-58. Scale bars are 20 μm in (a), (b) and (c), 500 nm in (d), 200 nm in (e), and 100 nm in (f).
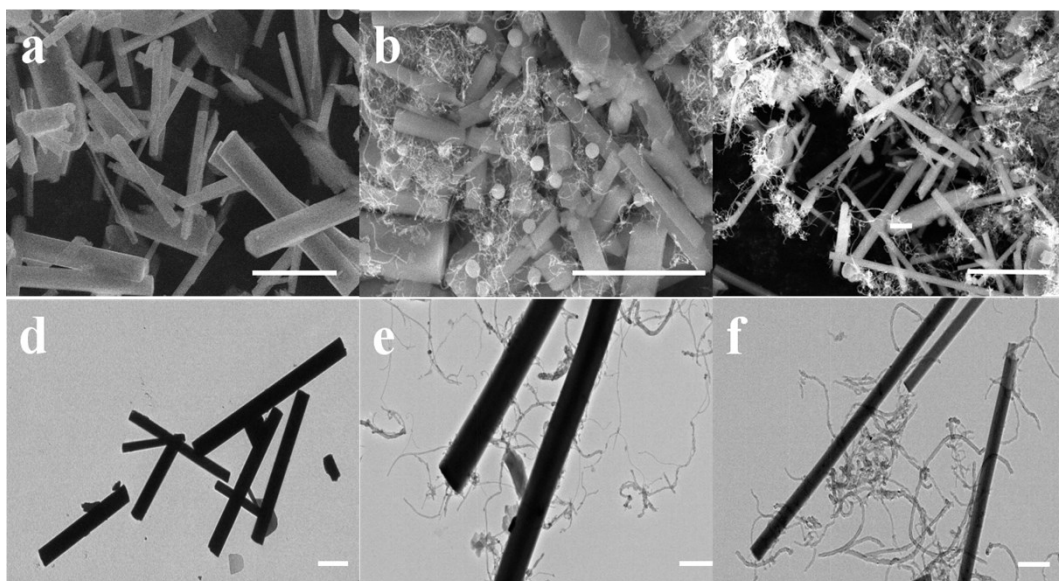
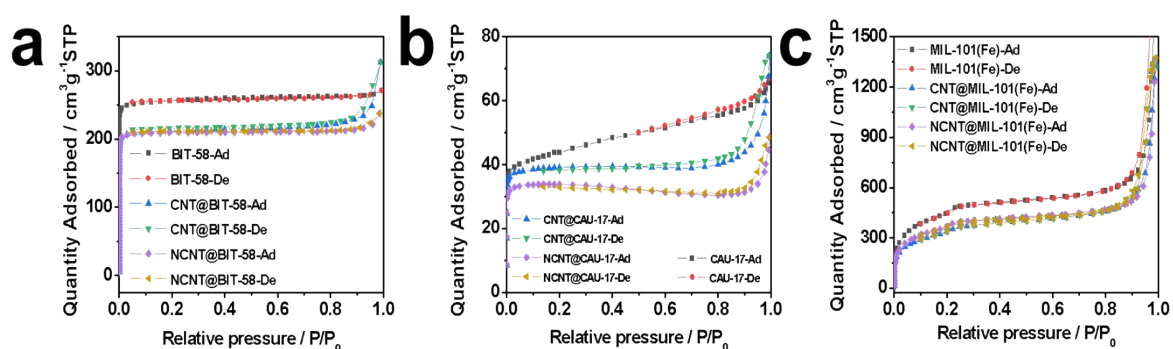**Fig. S3.** SEM images of (a) CAU-17, (b) CNT@CAU-17, (c) NCNT@CAU-17. TEM images of (e) CAU-17, (f) CNT@CAU-17, (g) NCNT@CAU-17. Scale bars are 5 μm in (a), 4 μm in (b), 5 μm in (c), 2 μm in (d), 500 nm in (e) and (f).
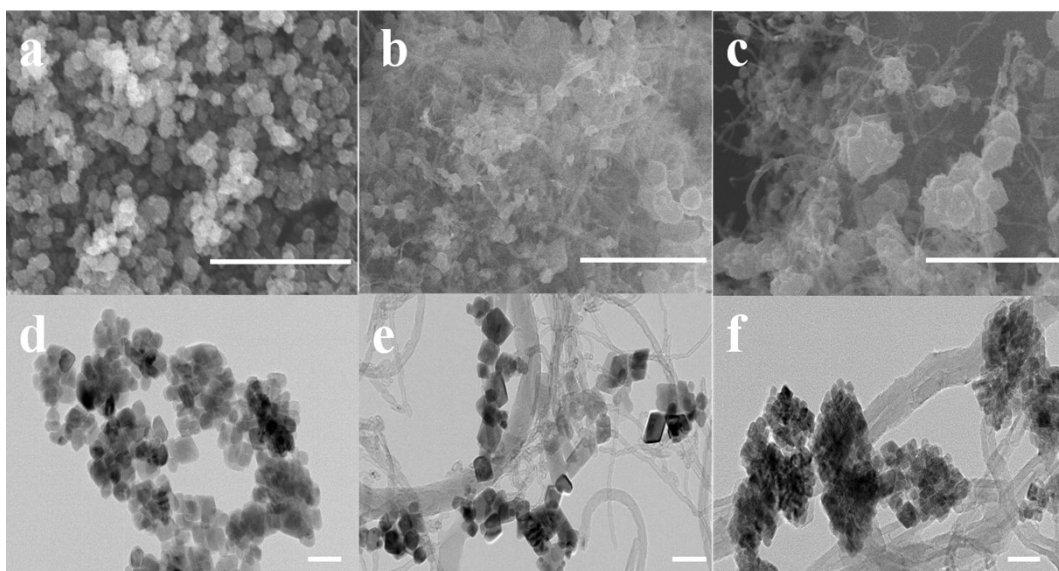
Fig. S4. SEM images of (a) MIL-101(Fe), (b) CNT@MIL-101(Fe), (c) NCNT@MIL-101(Fe). TEM images of (d) MIL-101(Fe), (e) CNT@MIL-101(Fe), (f) NCNT@MIL-101(Fe). Scale bars are 1 μm in (a), (b) and (c), 50 nm in (d), 100 nm in (e), and 50 nm in (f).

Fig. S5. N$_2$ adsorption-desorption isotherms of (a) BIT-58 system, (b) CAU-17 system and (c) MIL-101(Fe) system.
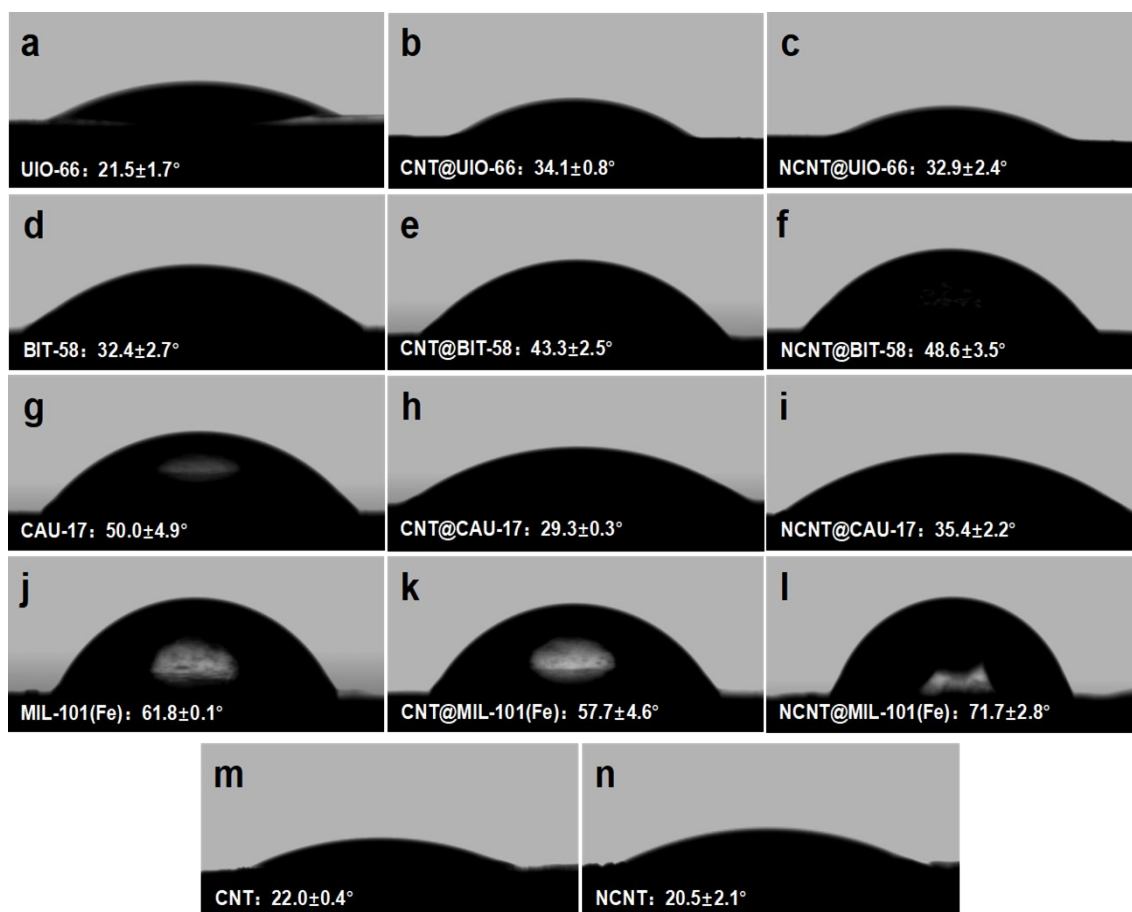
Fig. S6. Water contact angles image of (a-c) UIO-66 system, (d-f) BIT-58 system, (g-i) CAU-17 system, (j-l) MIL-101(Fe) system and (m-n) CNT/NCNT.
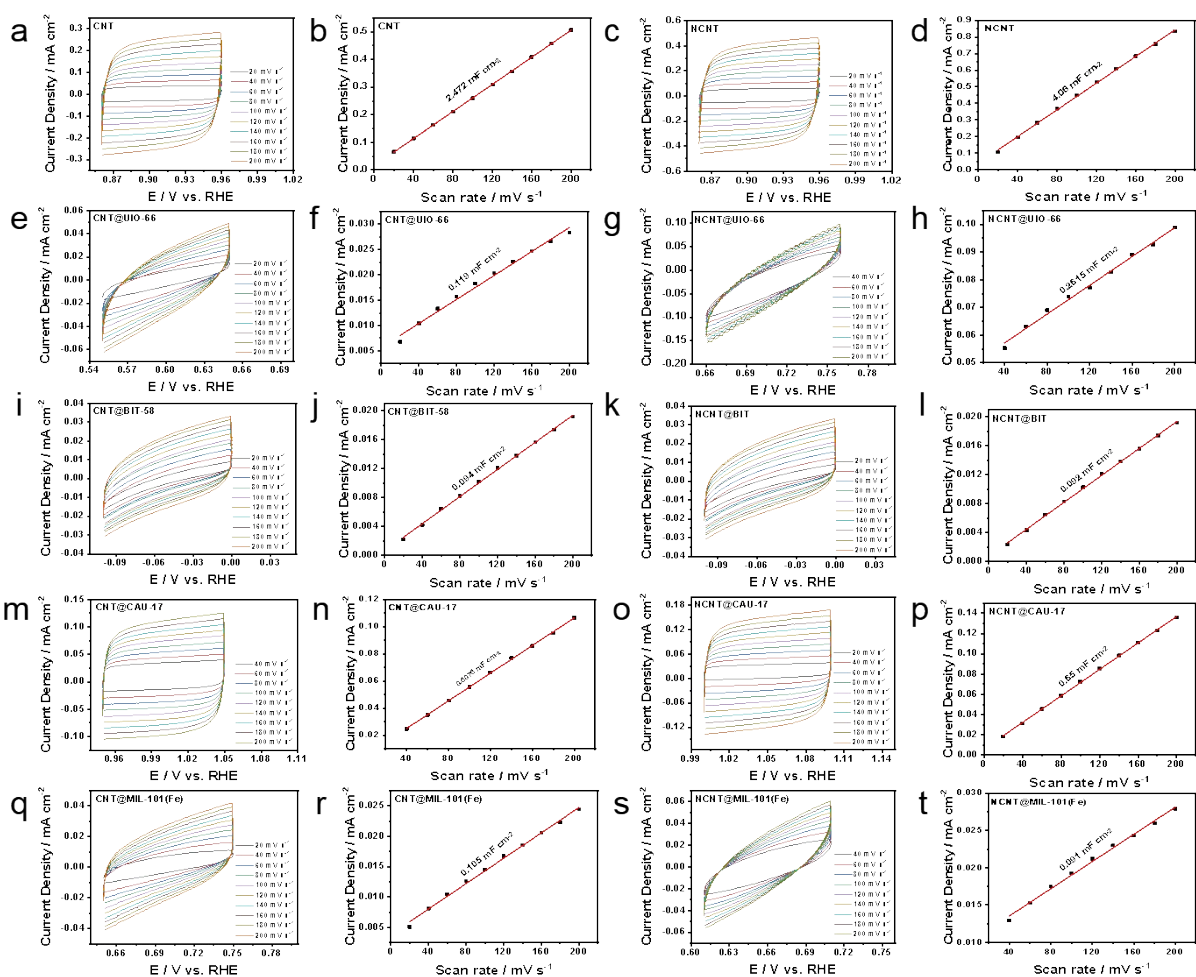
Fig. S7. CV curves of CNT/NCNT (a)/(c), CNT/NCNT@UIO-66 (e)/(g), CNT/NCNT@BIT-58 (i)/(k), CNT/NCNT@CAU-17 (m)/(o) and CNT/NCNT@MIL-101(Fe) (q)/(s). Capacitive current densities derived from CV curves against scan rates for CNT/NCNT (b)/(d), CNT/NCNT@UIO-66 (f)/(h), CNT/NCNT@BIT-58 (j)/(l), CNT/NCNT@CAU-17 (n)/(p) and CNT/NCNT@MIL-101(Fe) (r)/(t).
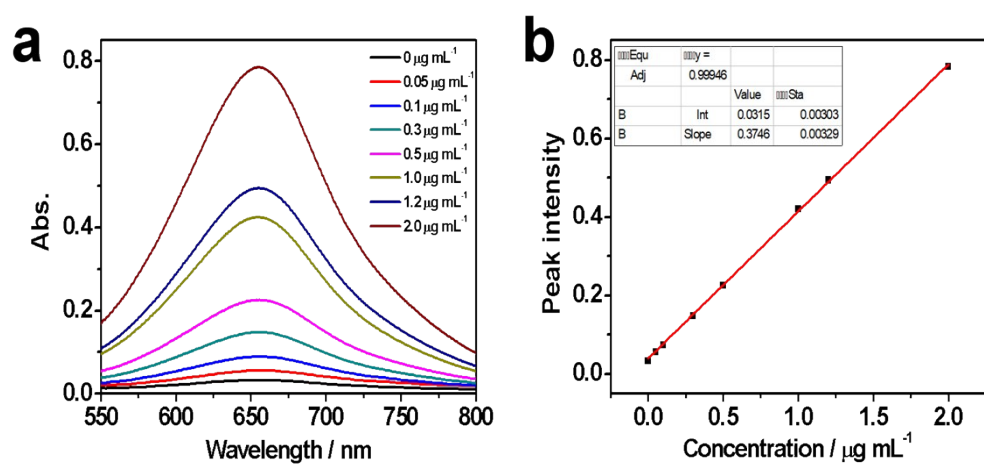
Fig. S8. (a) UV-Vis absorption spectra of indophenol blue solutions. (b) Calibration curve used for the estimation of NH^{4+} concentration. The 0.05 M H_2SO_4 was used as the baseline in the calibration curve.
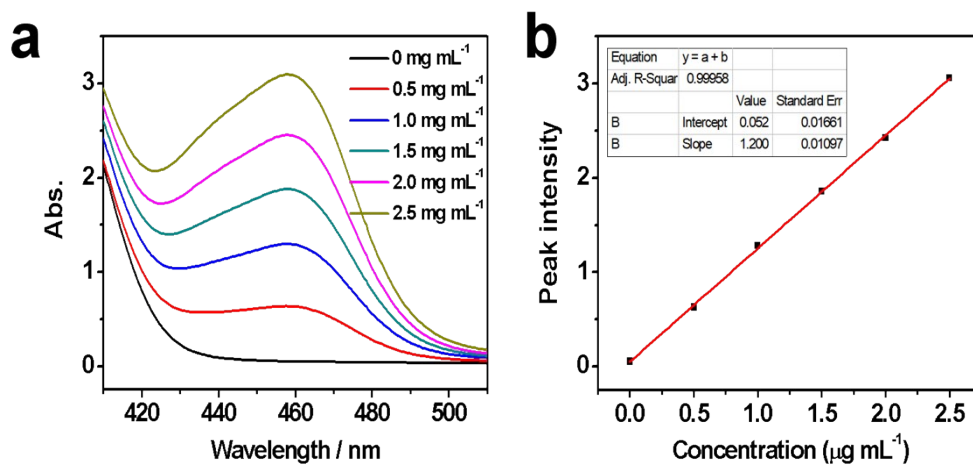

Fig. S9. (a) UV-vis absorption spectra and (b) corresponding standard calibration curve of the electrolytes of hydrazine.
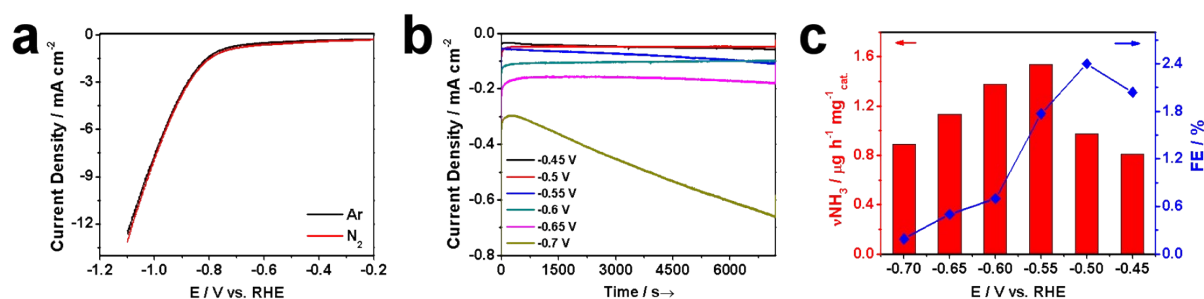

Fig. S10. (a) LSV curves of CNT under Ar and N_2. (b) Chronoamperometry tests for CNT at selected potentials. (c) UV-Vis absorption spectra of CNT at each potential. (d) NH_3 yield rates and corresponding FEs of CNT at selected potentials.
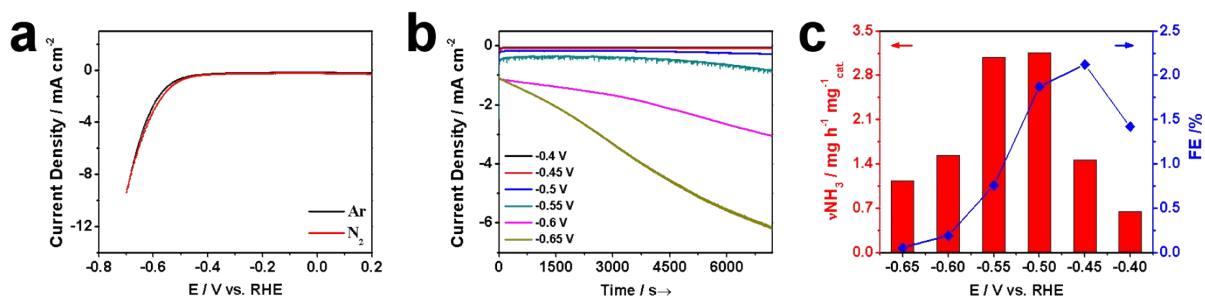
Fig. S11. (a) LSV curves of NCNT under Ar and N_2. (b) Chronoamperometry tests for NCNT at selected potentials. (c) UV-Vis absorption spectra of NCNT at each potential. (d) NH_3 yield rates and corresponding FEs of NCNT at selected potentials.
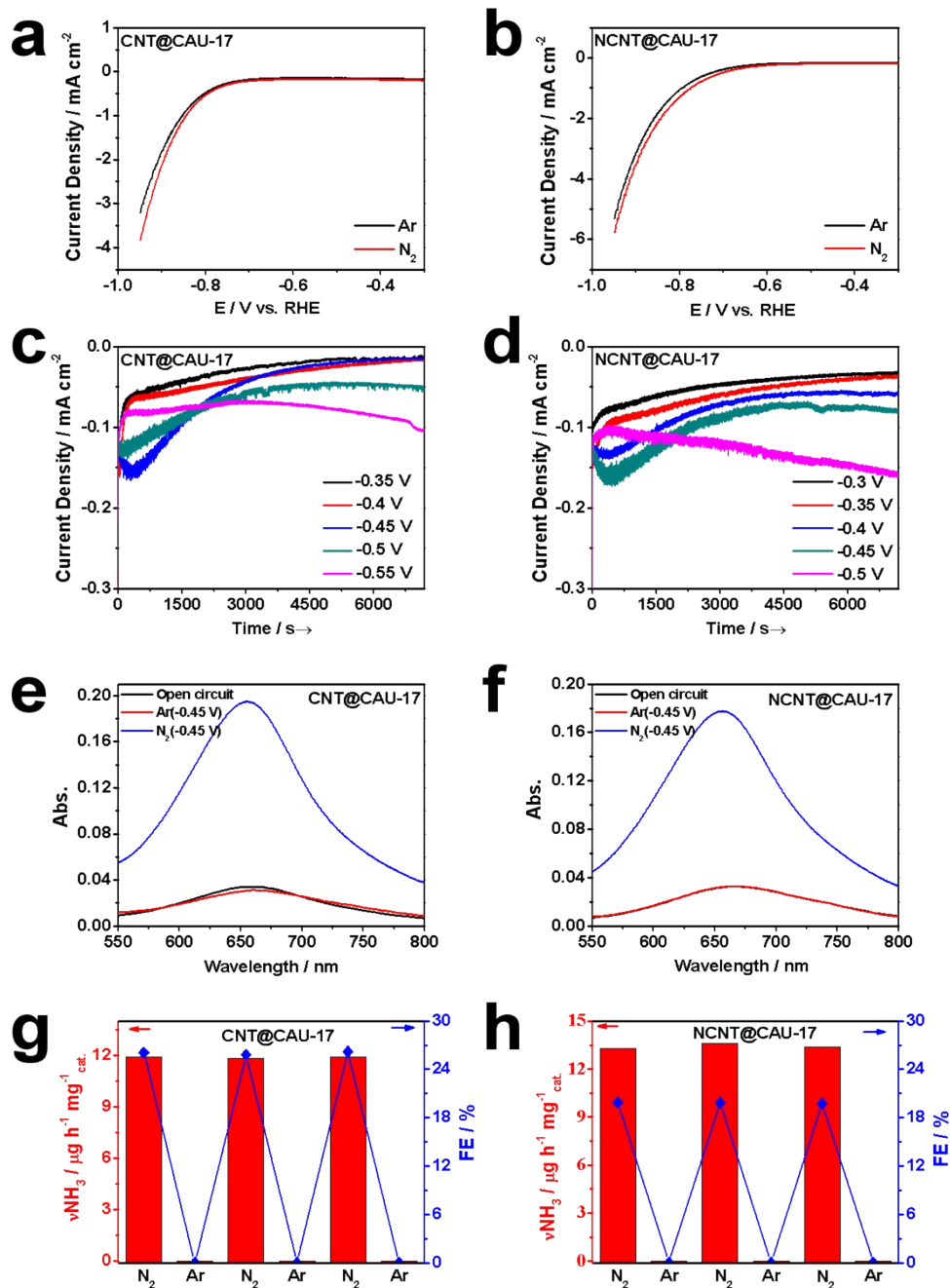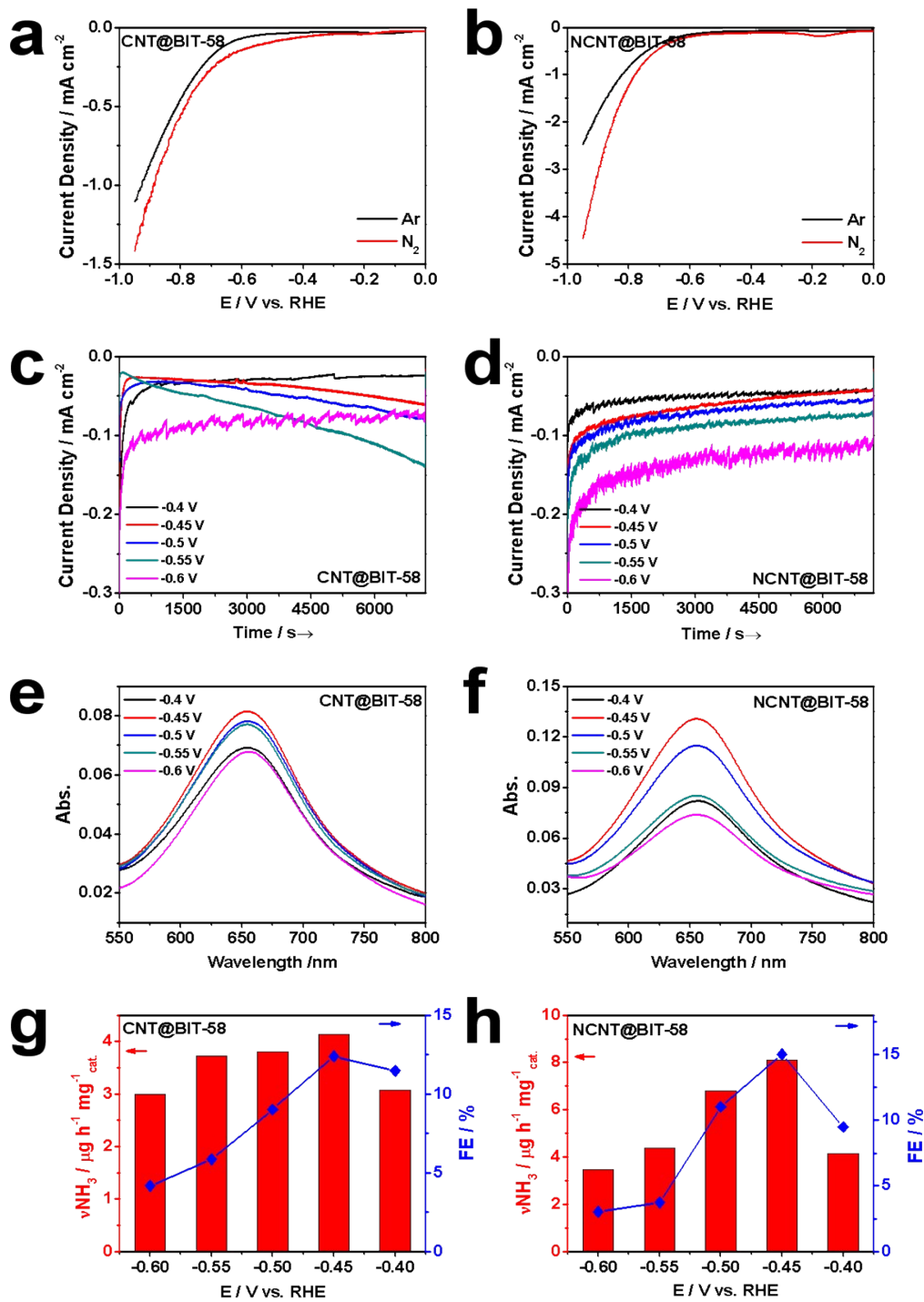
Fig. S12. (a), (b) Polarization curves of CNT/NCNT@CAU-17 under Ar and N_2. (c), (d) Potentialstatic curves of CNT/NCNT@CAU-17. (e), (f) UV-Vis absorption spectra of Ar-saturated post electrolytes under -0.45 V (red), N_2-saturated post electrolytes under open circuit potential (black) and N_2-saturated post electrolyte under -0.45 V (blue) of CNT/NCNT@CAU-17. (g), (h) NH_3 yield rates and corresponding FEs of CNT/NCNT@CAU-17 at -0.45 V with alternating 2 h cycles between N_2-saturated and Ar-saturated electrolytes, for a total of 12 h.
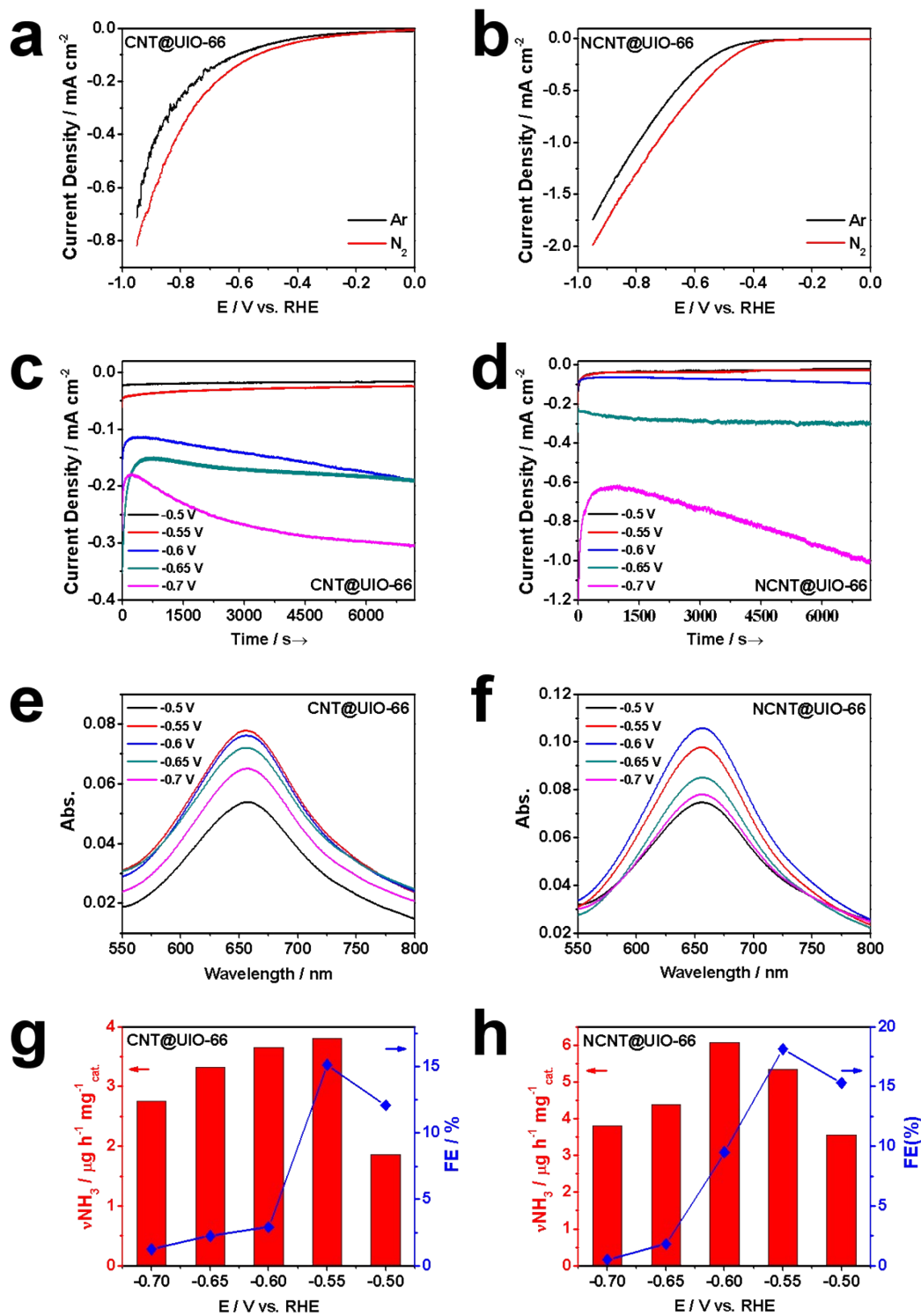
Fig. S13. (a), (b) Polarization curves of CNT/NCNT@UIO-66 under Ar and N_2. (c), (d) Potentialstatic curves of CNT/NCNT@UIO-66. (e), (f) UV-Vis absorption spectra of the electrolyte stained with indophenol blue indicator after electrolysis at selected potentials of CNT/NCNT@UIO-66. (g), (h) NH_3 yield rates and corresponding FEs of CNT/NCNT@UIO-66 at selected potentials.
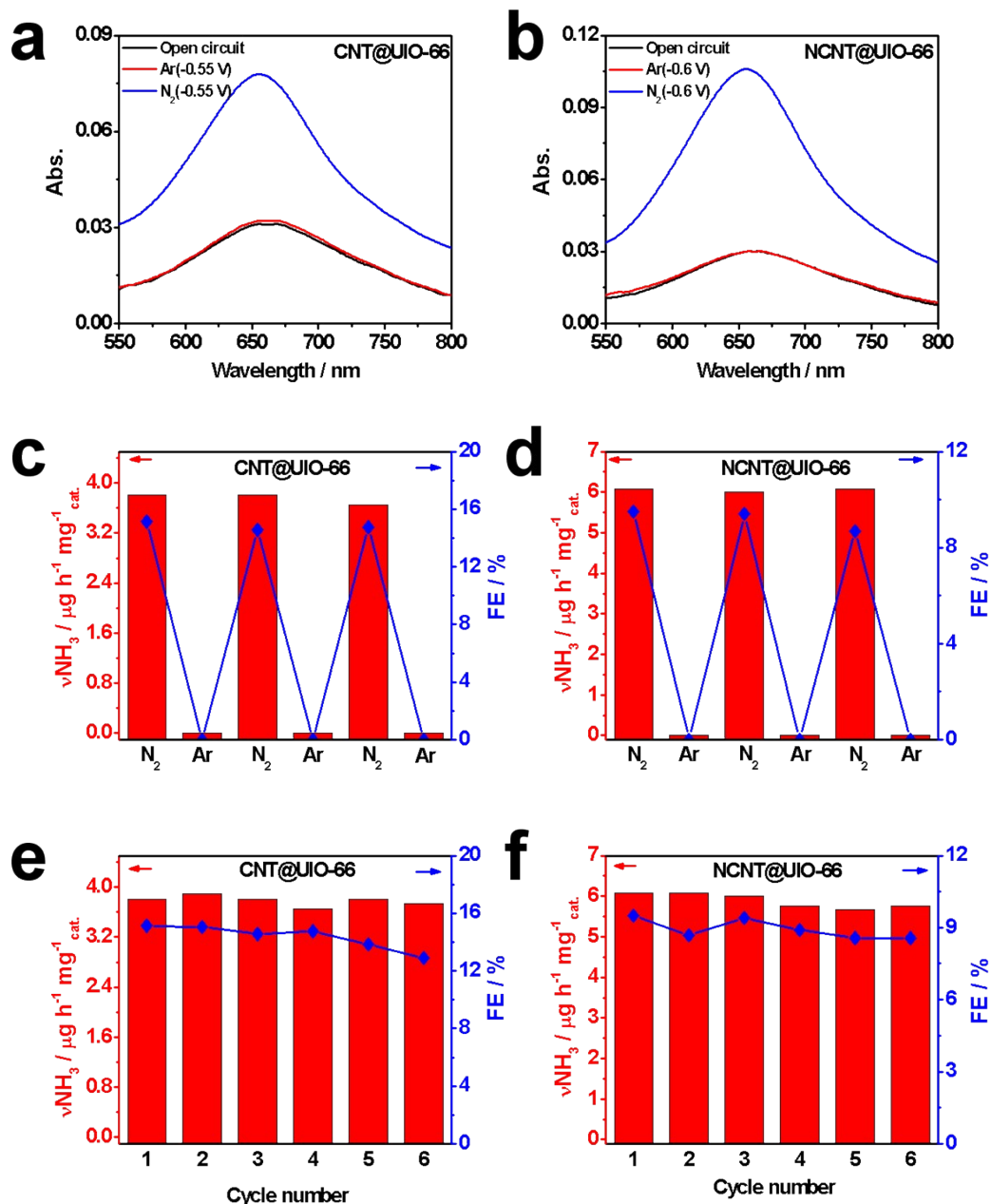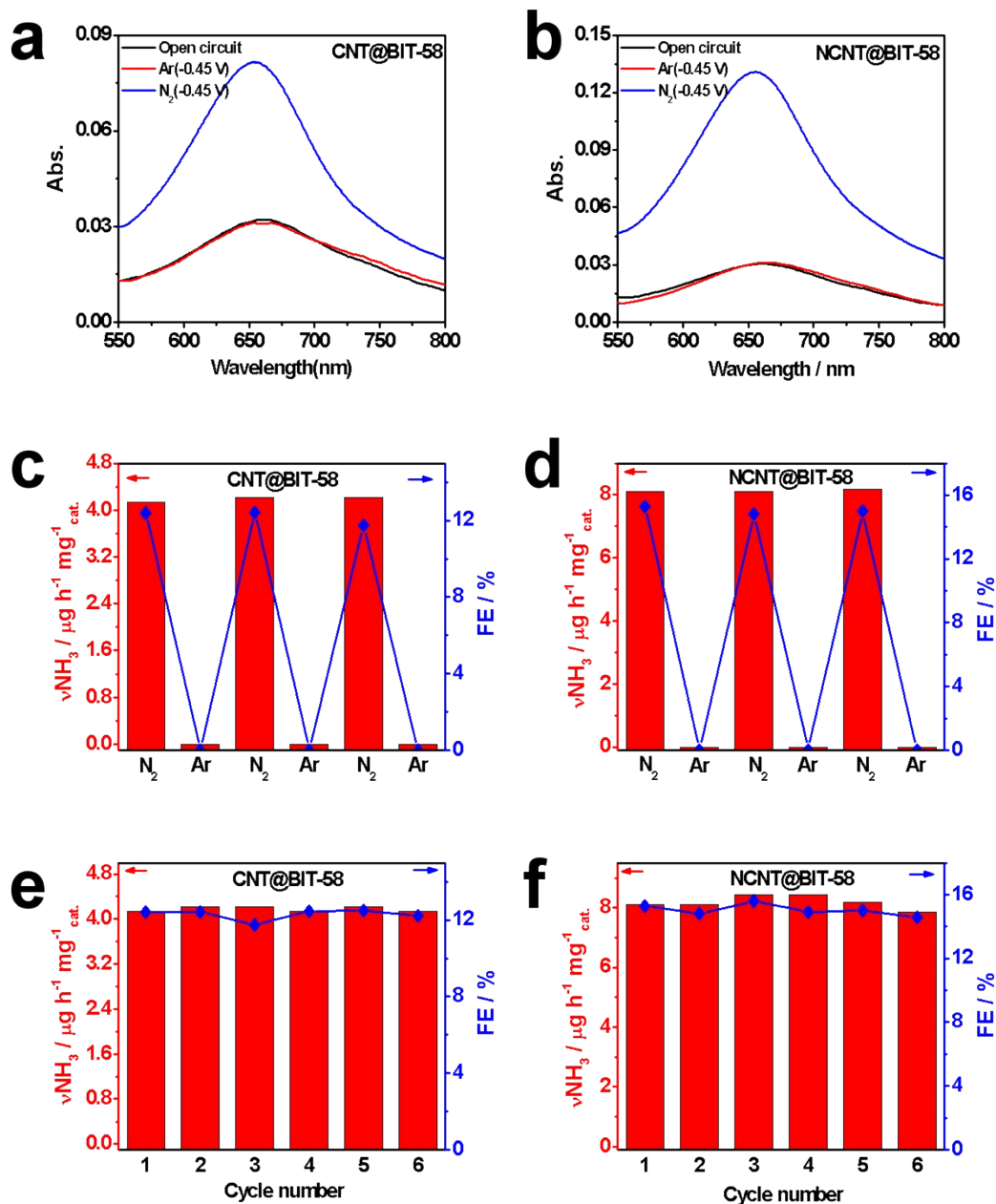
Fig. S14. (a), (b) UV-Vis absorption spectra of Ar-saturated post electrolytes under -0.55 V (red), N_2-saturated post electrolytes under open circuit potential (black) and N_2-saturated post electrolytes under -0.55 V (blue) of CNT/NCNT@UIO-66. (c), (d) NH_3 yield rates and corresponding FEs of CNT/NCNT@UIO-66 at -0.55 V with alternating 2 h cycles between N_2-saturated and Ar-saturated electrolytes, for a total of 12 h. (e), (f) NH_3 yield rates and corresponding FEs of CNT/NCNT@UIO-66 after each cycle at -0.55 V vs. RHE.
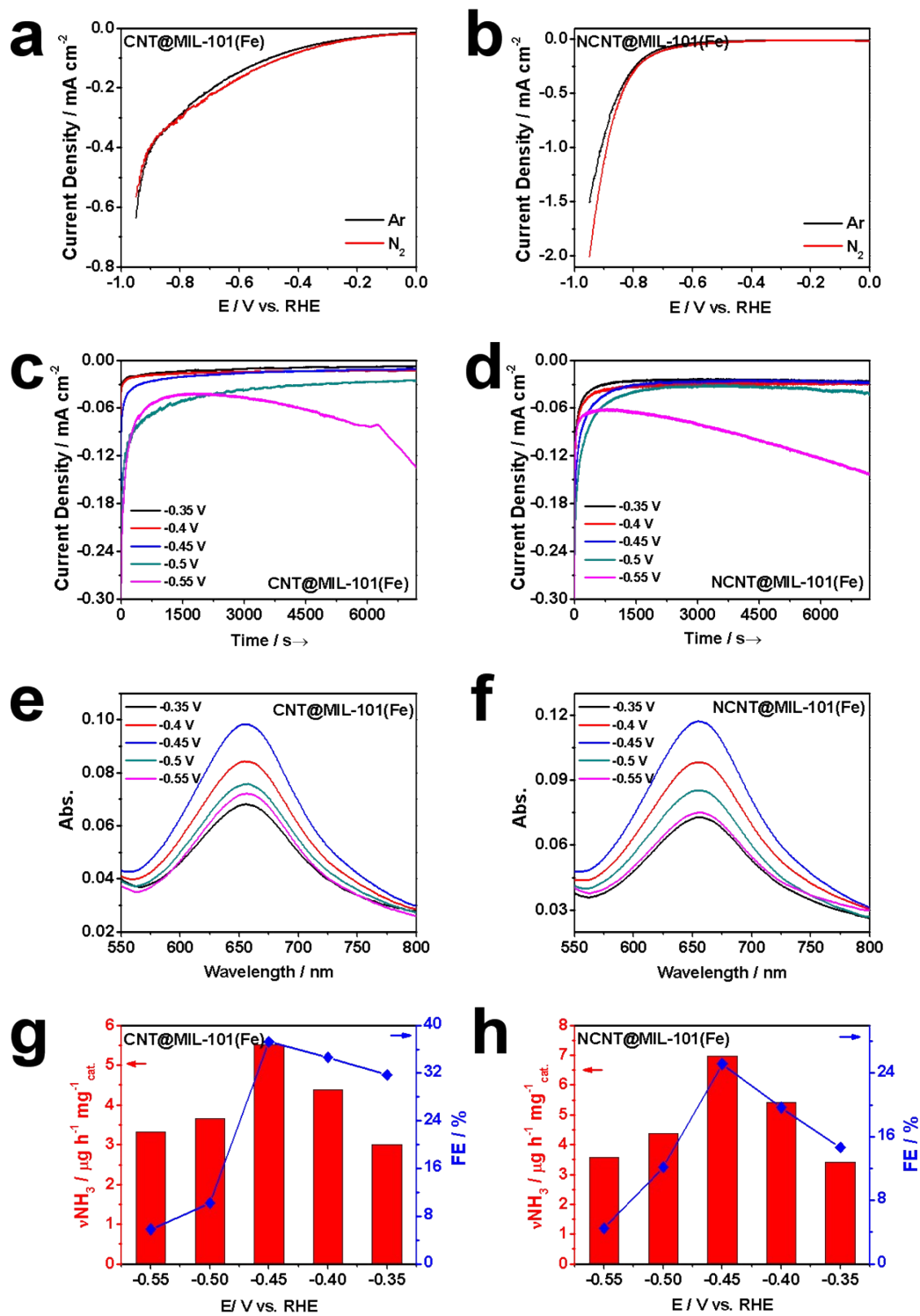
Fig. S15. (a), (b) Polarization curves of CNT/NCNT@BIT-58 under Ar and N_2. (c), (d) Potentialstatic curves of CNT/NCNT@BIT-58. (e), (f) UV-Vis absorption spectra of the electrolyte stained with indophenol blue indicator after electrolysis at selected potentials of CNT/NCNT@BIT-58. (g), (h) NH_3 yield rates and FEs corresponding of CNT/NCNT@BIT-58 at selected potentials.
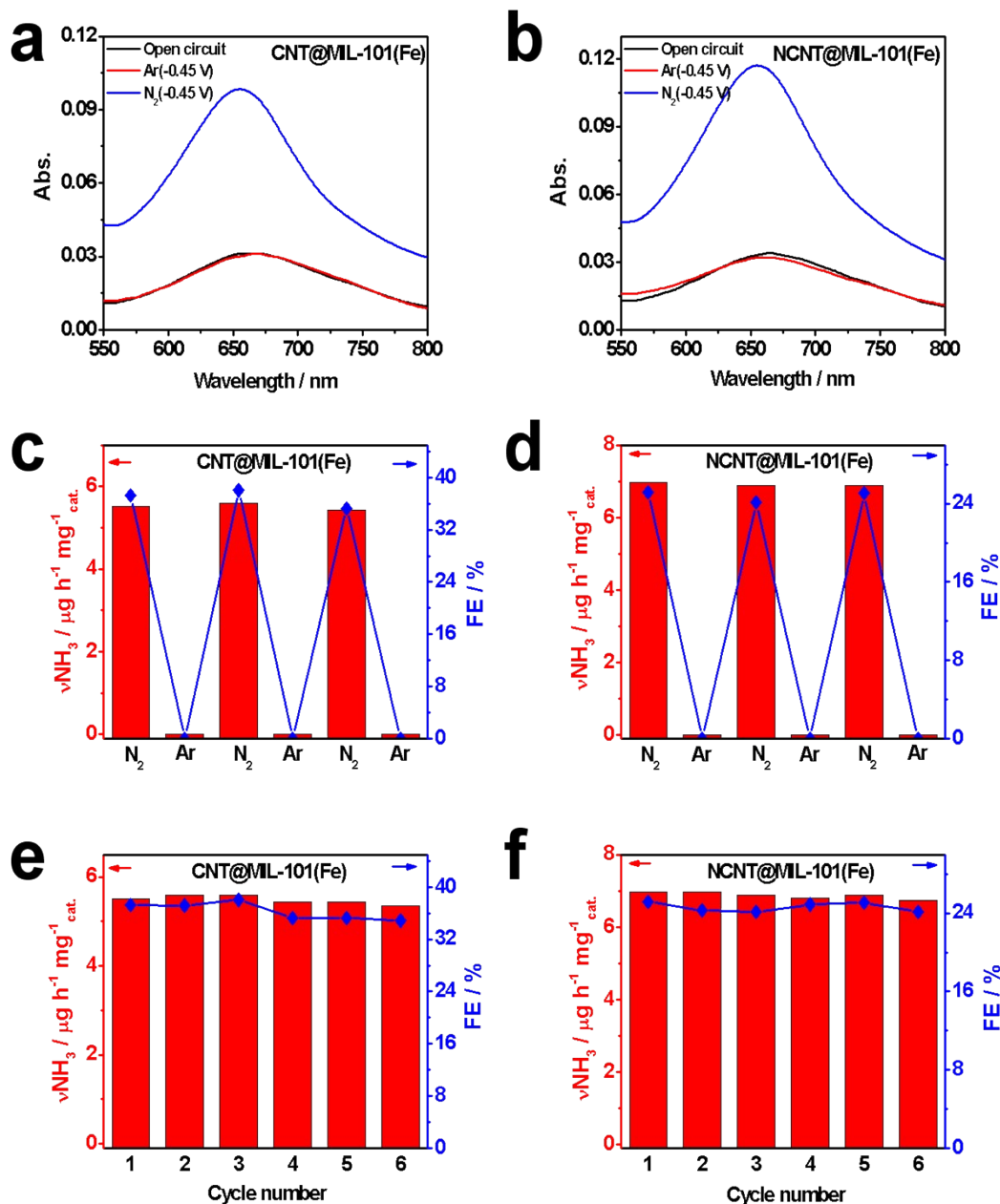
Fig. S16. (a), (b) UV-Vis absorption spectra of Ar-saturated post electrolytes under -0.45 V (red), N_2-saturated post electrolytes under open circuit potential (black) and N_2-saturated post electrolytes under -0.45 V (blue) of CNT/NCNT@BIT-58. (c), (d) NH_3 yield rates and corresponding FEs of CNT/NCNT@BIT-58 at -0.45 V with alternating 2 h cycles between N_2-saturated and Ar-saturated electrolytes, for a total of 12 h. (e), (f) NH_3 yield rates and corresponding FEs of CNT/NCNT@BIT-58 after each cycle at -0.45 V vs. RHE.

Fig. S17. (a), (b) Polarization curves of CNT/NCNT@MIL-101(Fe) under Ar and N_2. (c), (d) Potentialstatic curves of CNT/NCNT@MIL-101(Fe). (e), (f) UV-Vis absorption spectra of the electrolyte stained with indophenol blue indicator after electrolysis at selected potentials of CNT/NCNT@MIL-101(Fe). (g), (h) NH_3 yield rates and corresponding FEs of CNT/NCNT@MIL-101(Fe) at selected.

Fig. S18. (a), (b) UV-Vis absorption spectra of Ar-saturated post electrolytes under -0.45 V (red), N_2-saturated post electrolytes under open circuit potential (black) and N_2-saturated post electrolytes under -0.45 V (blue) of CNT/NCNT@MIL-101(Fe). (c), (d) NH_3 yield rates and corresponding FEs of CNT/NCNT@MIL-101(Fe) at -0.45 V with alternating 2 h cycles between N_2-saturated and Ar-saturated electrolytes, for a total of 12 h. (e), (f) NH_3 yield rates and corresponding FEs of CNT/NCNT@MIL-101(Fe) after each cycle at -0.45 V vs. RHE.
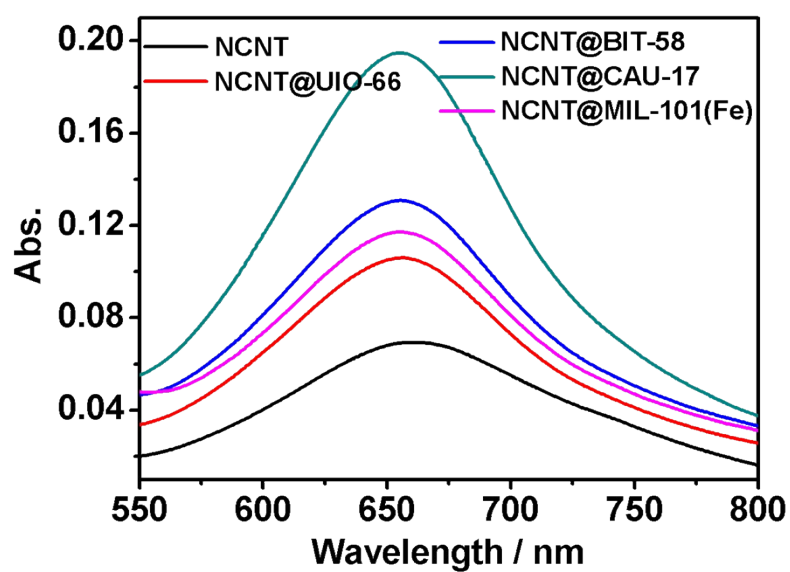
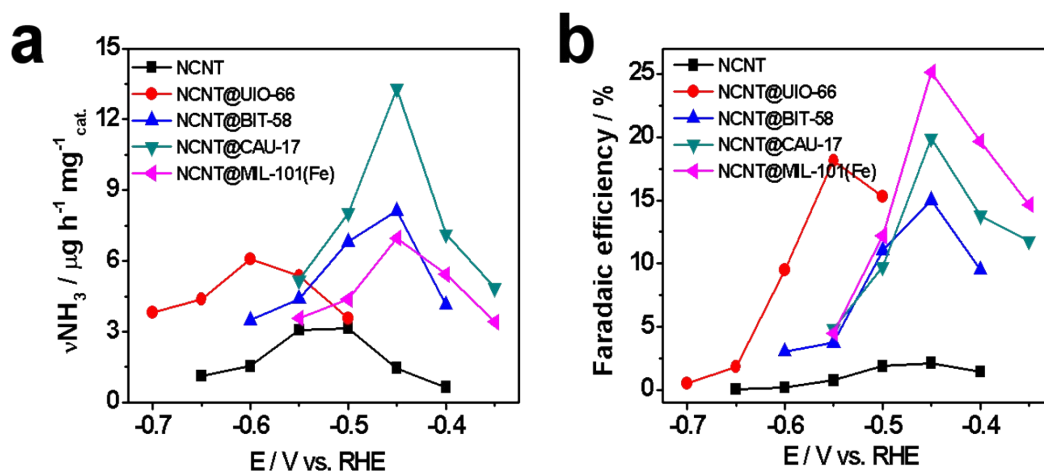**Fig. S19.** The highest UV-Vis absorption spectra of each NCNT@MOF catalyst.

Fig. S20. (a) NH$_3$ yield rates of NCNT@MOFs at selected potentials. (b) Corresponding FEs of NCNT@MOFs.
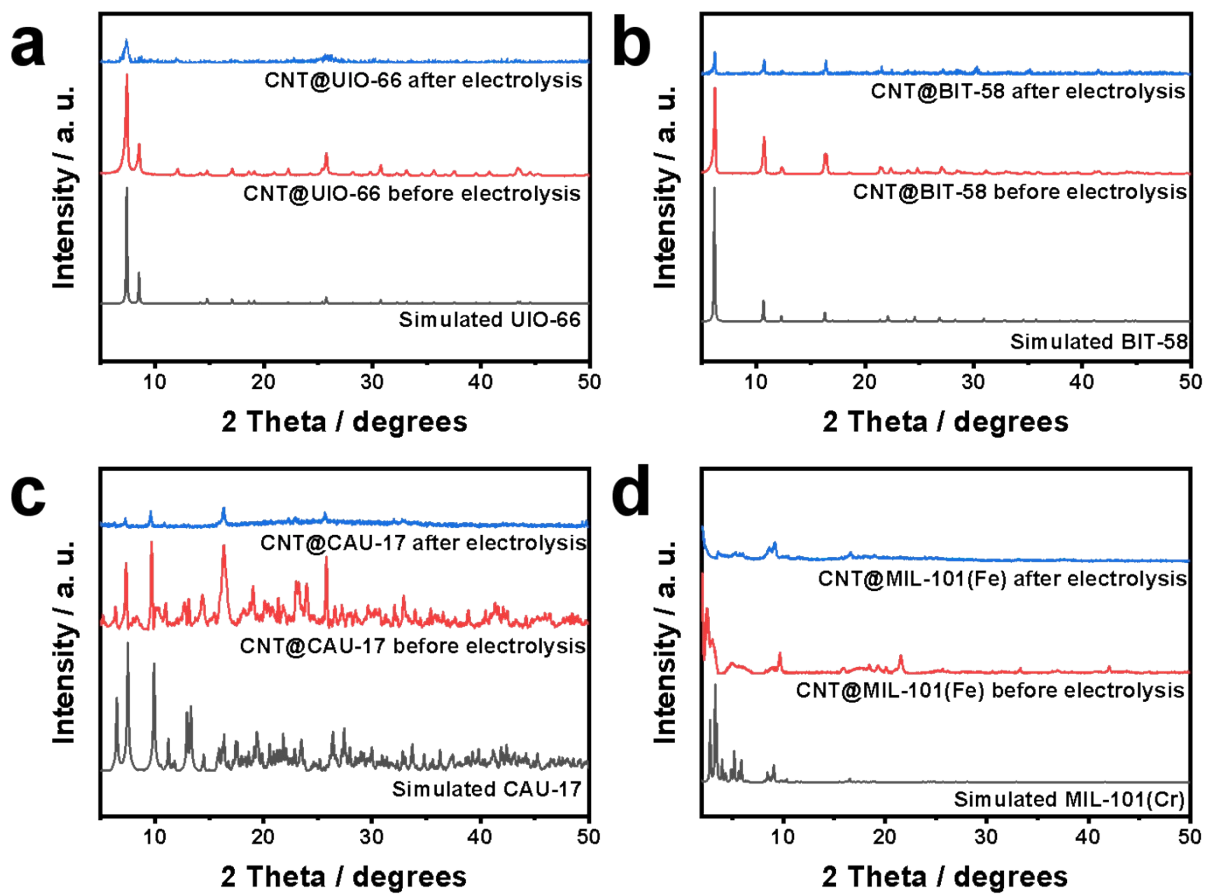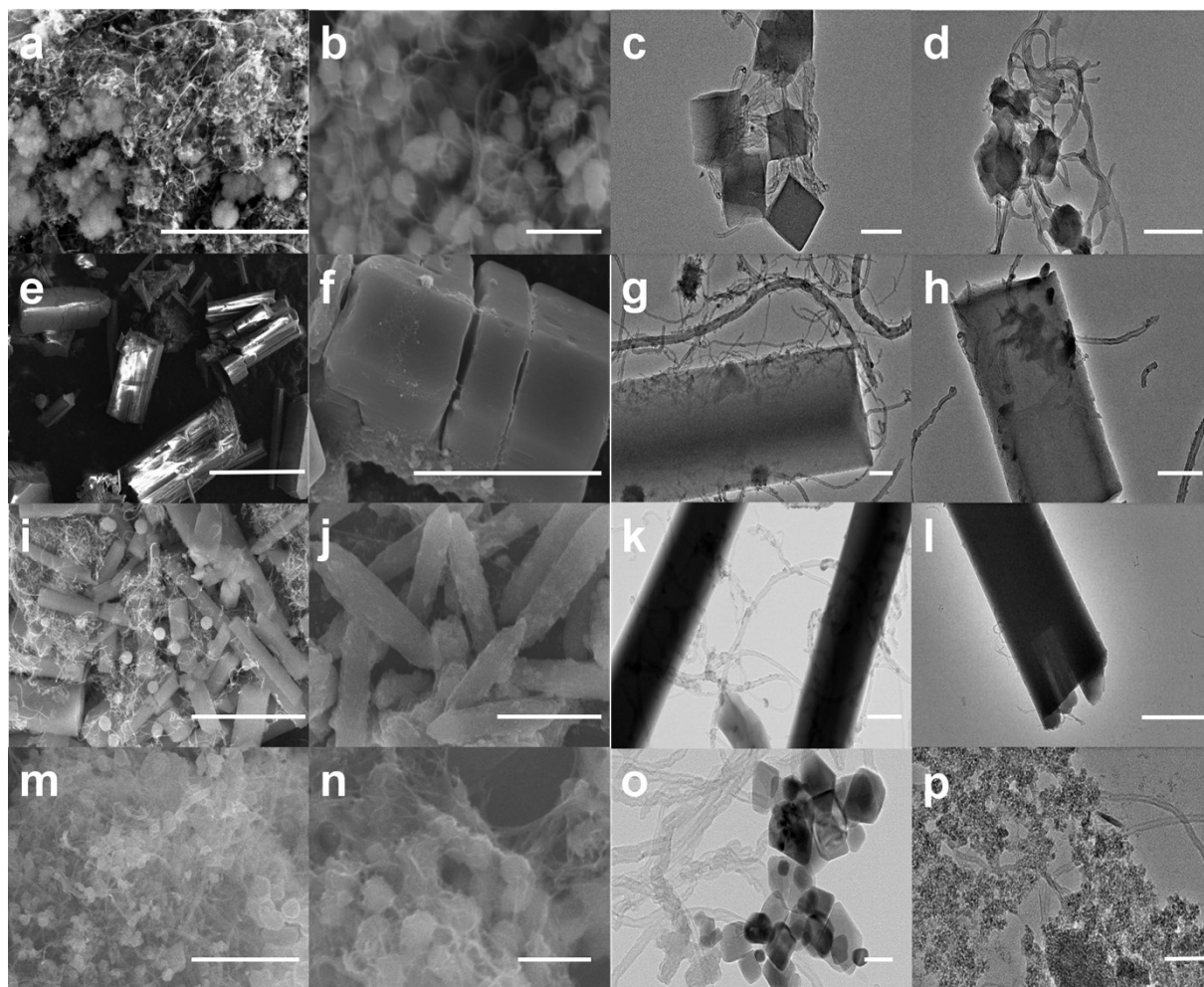
Fig. S21. XRD patterns of CNT@MOFs after electrolysis 6 cycles at carbon paper.

Fig. S22. SEM/TEM images of CNT@UIO-66 before (a)/(c) and after (b)/(d) electrolysis 6 cycles, CNT@BIT-58 before (e)/(g) and after (f)/(h) electrolysis 6 cycles, CNT@CAU-17 before (i)/(k) and after (j)/(l) electrolysis 6 cycles, CNT@MIL-101(Fe) before (m)/(o) and after (n)/(p) electrolysis 6 cycles. Scar bar are 3 μm in (a), 500 nm in (b), (k), (l), (n), 100 nm in (c), (o), (p), 200 nm in (d), (g), (h), 20 μm in (e), 5 μm in (f), 200 nm in (g), (h), 4μm in (i), 2 μm in (j), 1 μm in (m).
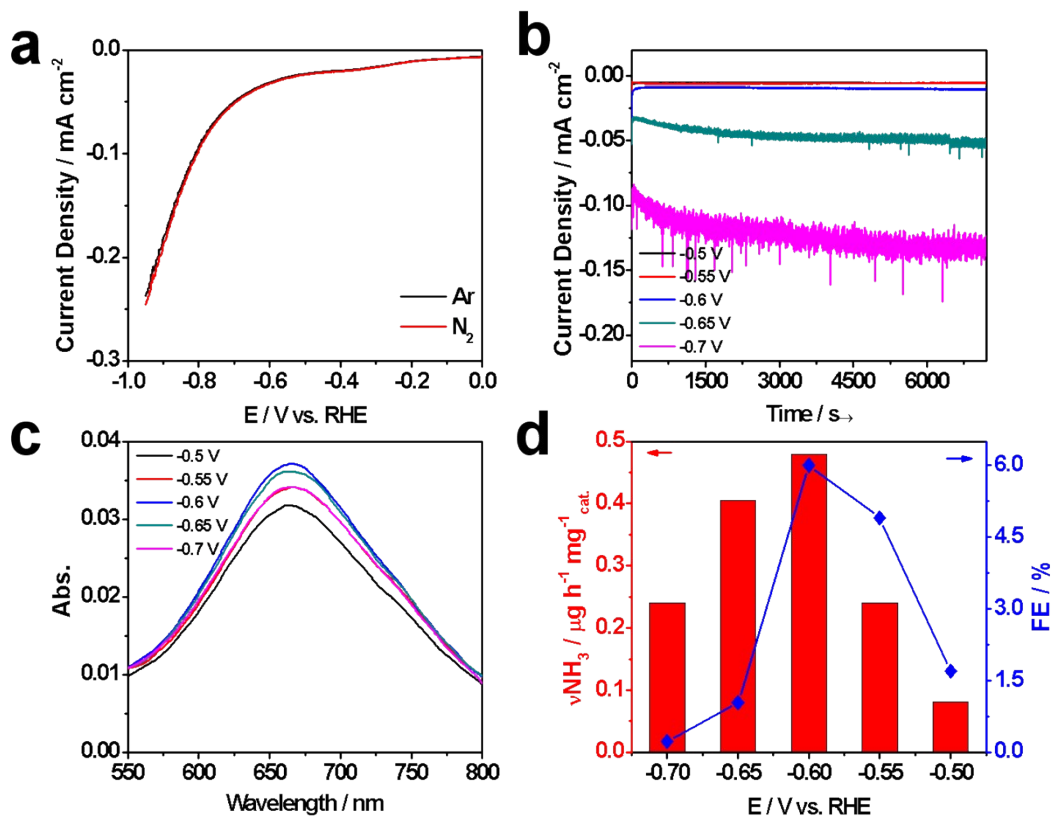
Fig. S23. (a) Polarization curves of pure UIO-66 under Ar and N_2. (b) Potentialstatic curves of pure UIO-66. (c) UV-Vis absorption spectra of the electrolyte stained with indophenol blue indicator after electrolysis at selected potentials of pure UIO-66. (d) NH_3 yield rates and corresponding FEs of pure UIO-66.
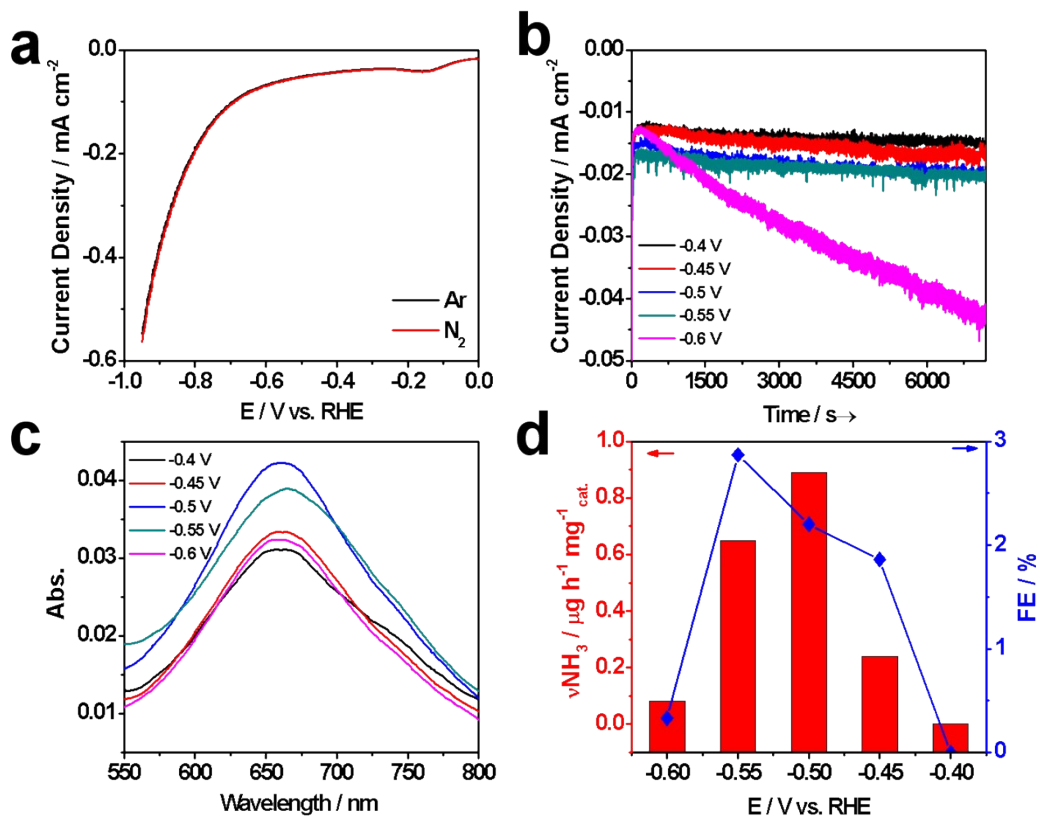
Fig. S24. (a) Polarization curves of pure BIT-58 under Ar and N_2. (b) Potentialstatic curves of pure BIT-58. (c) UV-Vis absorption spectra of the electrolyte stained with indophenol blue indicator after electrolysis at selected potentials of pure BIT-58. (d) NH_3 yield rates and corresponding FEs of pure BIT-58.
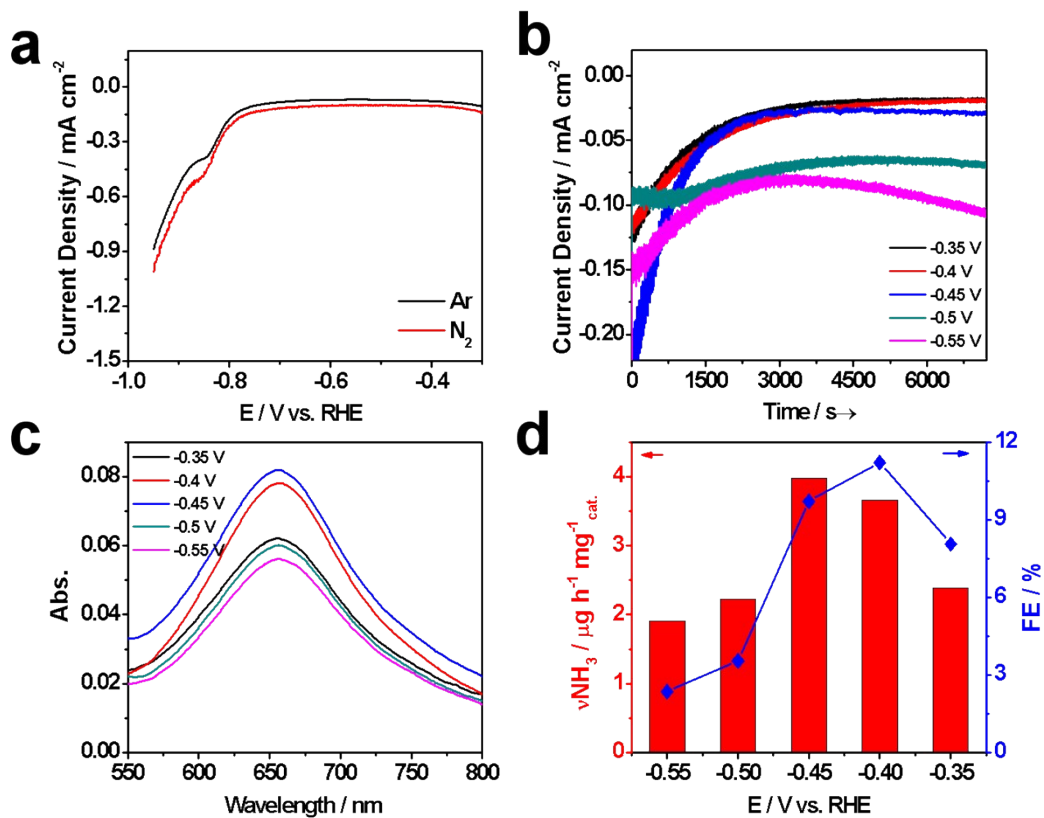
Fig. S25. (a) Polarization curves of pure CAU-17 under Ar and N_2. (b) Potentialstatic curves of pure CAU-17. (c) UV-Vis absorption spectra of the electrolyte stained with indophenol blue indicator after electrolysis at selected potentials of pure CAU-17. (d) NH_3 yield rates and corresponding FEs of pure CAU-17.

Fig. S26. (a) Polarization curves of pure MIL-101(Fe) under Ar and N_2. (b) Potentialstatic curves of pure MIL-101(Fe). (c) UV-Vis absorption spectra of the electrolyte stained with indophenol blue indicator after electrolysis at selected potentials of pure MIL-101(Fe). (d) NH_3 yield rates and corresponding FEs of pure MIL-101(Fe).
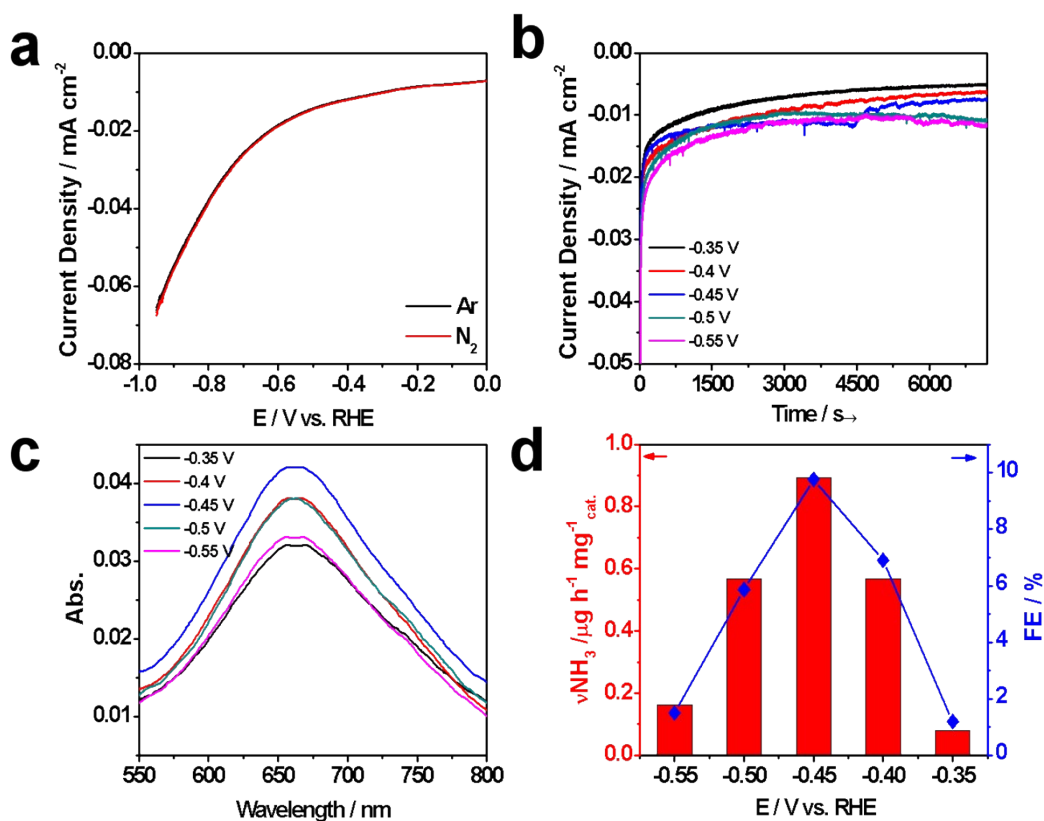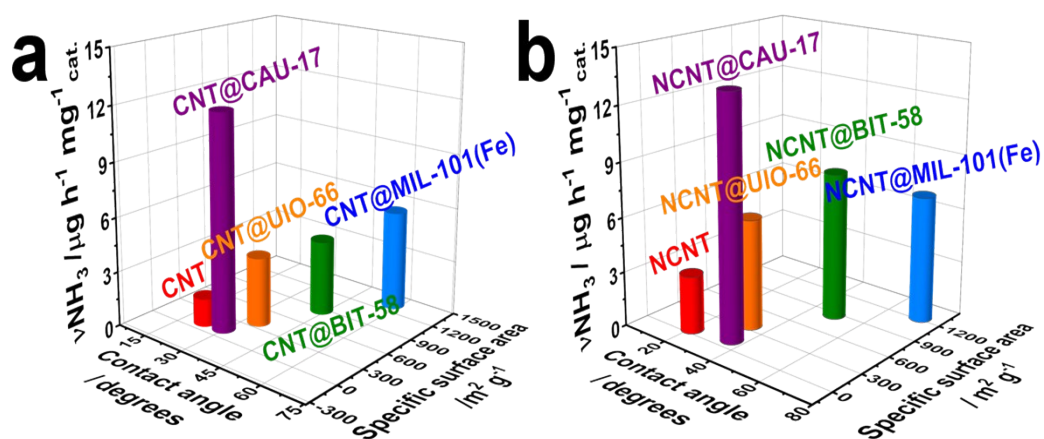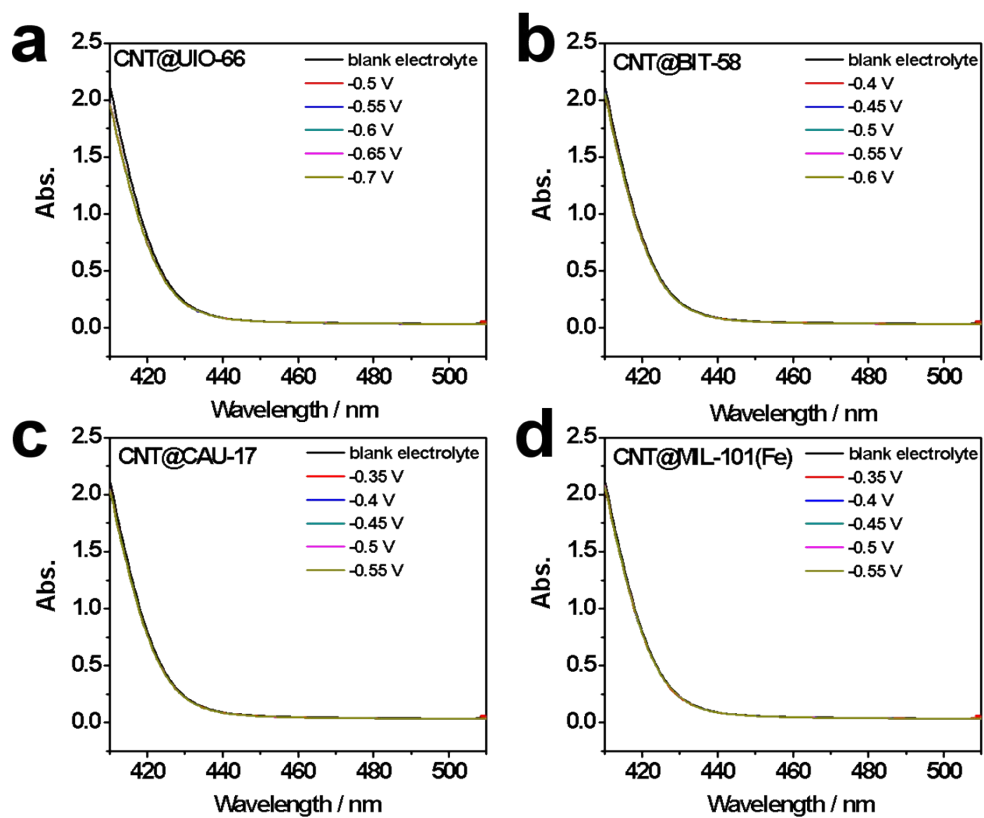

Fig. S27. (a), (b) The optimal NH_3 yield rates of CNT/NCNT@MOFs over different water contact angles and specific surface areas.

Fig. S28. UV-vis absorption spectra of the 0.05 M H_2SO_4 electrolyte after electrolysis on (a) CNT@UIO-66, (b) CNT@BIT-58, (c) CNT@CAU-17 and (d) CNT@MIL-101(Fe) electrodes stained with N_2H_4 color indicator after charging at selected potentials for 2 h under ambient conditions.
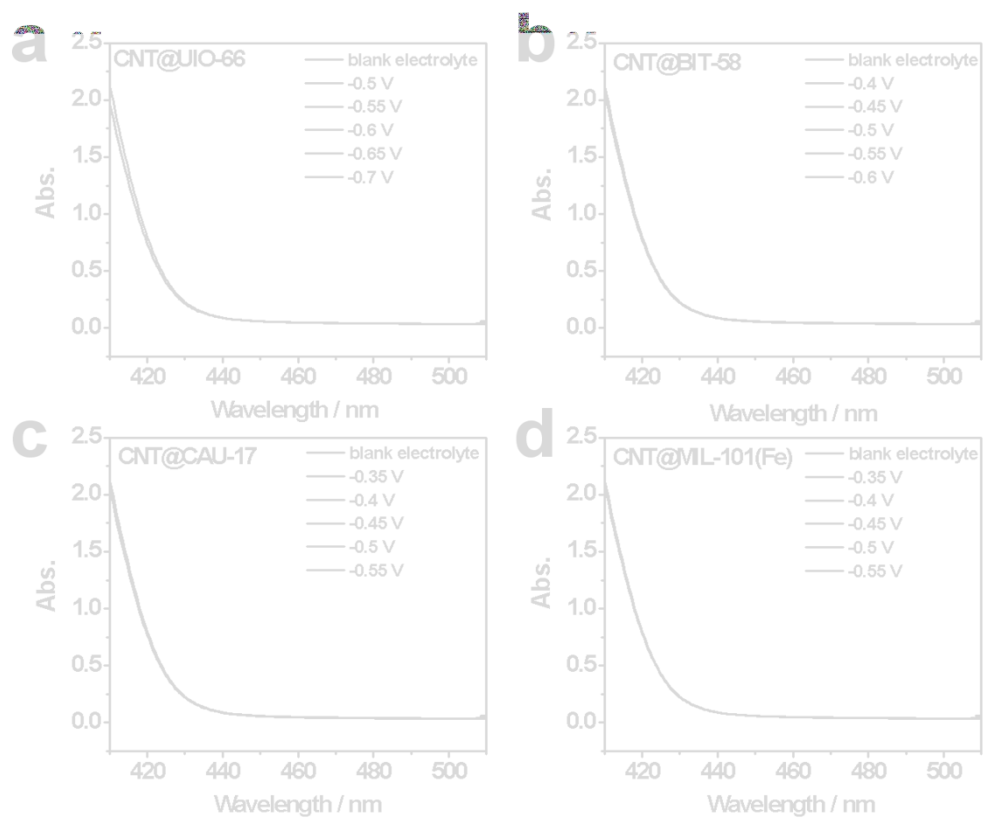
Fig. S29. UV-vis absorption spectra of the 0.05 M H_2SO_4 electrolyte after electrolysis on (a) NCNT@UIO-66, (b) NCNT@BIT-58, (c) NCNT@CAU-17 and (d) NCNT@MIL-101(Fe) electrodes stained with N_2H_4 color indicator after charging at selected potentials for 2 h under ambient conditions.
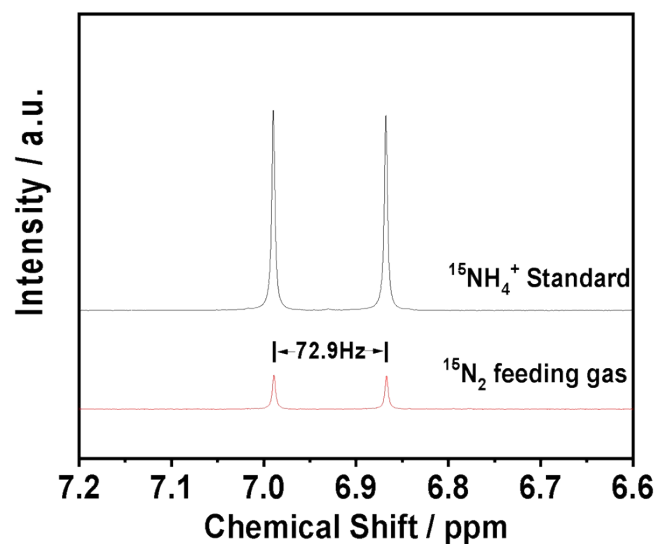
Fig. S30. ^{1}H NMR spectra for the electrolyte of NCNT@CAU-17 after 2h electrolysis with $^{15}N_2$ as the feeding gas, and the corresponding standard solution.

Table S1. Specific surface areas of CNT/NCNT and CNT/NCNT@MOFs.

Catalyst	Specific surface area / $m^2\ g^{-1}$	Catalyst	Specific surface area / $m^2\ g^{-1}$
CNT	127.6	NCNT	56.5
CNT@CAU-17	133.3	NCNT@CAU-17	114.1
CNT@UIO-66	395.8	NCNT@UIO-66	361.1
CNT@BIT-58	879.1	NCNT@BIT-58	874.3
CNT@MIL-101(Fe)	1332.9	NCNT@MIL-101(Fe)	1233.2

Table S2. Comparison of the electrochemical NRR activities for CNT/NCNT@MOFs with other carbon-based catalysts under ambient conditions.

Catalyst	Electrolyte	Potential/V vs. RHE	NH_3 yield rate / $\mu g\ h^{-1}\ mg^{-1}_{cat.}$	FE/%	Reference
CNT@UIO-66 NCNT@UIO-66	0.05 M H_2SO_4	-0.55; $v NH_3$: -0.6 FE: -0.55	3.811 (2.64 x $10^{-4}\ \mu g\ cm^{-2}\ s^{-1}$) 6.081 (4.22 x $10^{-4}\ \mu g\ cm^{-2}\ s^{-1}$)	15.14 18.13	**This work**
CNT@BIT-58 NCNT@BIT-58	0.05 M H_2SO_4	-0.45	4.135 (2.87 x $10^{-4}\ \mu g\ cm^{-2}\ s^{-1}$) 8.108 (5.63 x $10^{-4}\ \mu g\ cm^{-2}\ s^{-1}$)	12.4 15.03	**This work**
CNT@CAU-17 NCNT@CAU-17	0.05 M H_2SO_4	$v NH_3$: -0.45 FE: -0.55; -0.45	11.92 (8.27 x $10^{-4}\ \mu g\ cm^{-2}\ s^{-1}$) 13.3 (9.24 x $10^{-4}\ \mu g\ cm^{-2}\ s^{-1}$)	31.27 19.9	**This work**
CNT@MIL-101(Fe) NCNT@MIL-101(Fe)	0.05 M H_2SO_4	-0.45	5.5135 (3.83 x $10^{-4}\ \mu g\ cm^{-2}\ s^{-1}$) 6.97 (4.84 x $10^{-4}\ \mu g\ cm^{-2}\ s^{-1}$)	37.28 25.15	**This work**
B_4C	0.1 M HCl	-0.75	7.38 x $10^{-4}\ \mu g\ cm^{-2}\ s^{-1}$	15.95	5
B_4C-BGQDs/CPE	0.1 M HCl	$v NH_3$: -0.45 FE: -0.35	28.6	16.7	8
B-doped graphene	0.05 M H_2SO_4	-0.5	1.361 x $10^{-3}\ \mu g\ cm^{-2}\ s^{-1}$	10.8	9
O-CNT/CP	0.1 M $LiClO_4$	-0.4	33.23	12.5	10
TiC/C	0.1 M HCl	-0.5	14.1	5.8	11
CC-450	0.1 M Na_2SO_4 + 0.02 M H_2SO_4	-0.3	4.403 x $10^{-4}\ \mu g\ cm^{-2}\ s^{-1}$	6.92	12
NPC	0.1 M HCl	-0.2	0.97	4.2	13
PCN-NV4	0.1 M HCl	-0.2	8.09	11.59	14
N-doped porous carbon-500	0.005 M H_2SO_4	-0.1	6.19 x $10^{-3}\ \mu g\ cm^{-2}\ s^{-1}$	9.98	15
S-doped carbon nanosphere	0.1 M Na_2SO_4	-0.4	5.30 x $10^{-4}\ \mu g\ cm^{-2}\ s^{-1}$	7.47	16
N-doped porous carbon-750	0.05 M H_2SO_4	-0.9	3.97 x $10^{-3}\ \mu g\ cm^{-2}\ s^{-1}$	1.42	17

Table S3. Summary of characterization data and eNRR activities for CNTs@MOFs.

Catalyst	Specific surface area / $m^2 g^{-1}$	Contact angle / degrees	NH_3 yield rate / $\mu g\ h^{-1}\ mg^{-1}_{cat.}$	NH_3 yield rate / $\mu g\ h^{-1}\ mg^{-1}_{CNT/NCNT}$	FE/%
CNT	127.6	22.0±0.4	1.54	1.54	1.77
CNT@CAU-17	133.3	29.3±0.3	11.92	61.24	31.27
CNT@UIO-66	395.8	34.1±0.8	3.811	115.0	15.14
CNT@BIT-58	879.1	43.3±2.5	4.135	184.69	12.4
CNT@MIL-101(Fe)	1332.9	57.7±4.6	5.5135	461.81	37.28
NCNT	56.5	20.5±2.1	3.16	3.16	1.87
NCNT@CAU-17	114.1	35.4±2.2	13.3	71.88	19.9
NCNT@UIO-66	361.1	32.9±2.4	6.081	180.38	18.13
NCNT@BIT-58	874.3	48.6±3.5	8.108	373.08	15.04
NCNT@MIL-101(Fe)	1233.2	71.7±2.8	6.97	607.35	25.15

Reference

1 J. H. Cavka, S. Jakobsen, U. Olsbye, N. Guillou, C. Lamberti, S. Bordiga and K. P. Lillerud, *J. Am. Chem. Soc.,* 2008, **130**, 13850-13851.

2 I. A. Ken, K. Milan, J. Su, F. Mark, H. Y. Xu, X. D. Zou, O. Michael and S. Norbert, *J. Am. Chem. Soc.,* 2016, **138**, 1970-1976.

3 Y. F. Chen, S. H. Zhang, F. Chen, S. J. Cao, Y. Cai, S. Q. Li, H. W. Ma, X. J. Ma, P. F. Li, X. Q. Huang and B. Wang, *J. Mater. Chem. A,* 2018, **6**, 342-348.

4 J. Shin, M. Kim, J. Cirera, S. Chen, G. Y. Halder, T. A. Yersak, F. Paesani, S. M. Cohen and Y. S. Meng, *J. Mater. Chem. A,* 2015, **3**, 4738-4744.

5 W. B. Qiu, X. Y. Xie, J. D. Qiu, W. H. Fang, R. P. Liang, X. Ren, X. Q. Ji, G. W. Cui, A. M. Asiri, G. L. Cui, B. Tang and X. P. Sun, *Nat. Commun.*, 2018, **9**, 1-8.

6 D. Zhu, L. Zhang, R. E. Ruther and R. J. Hamers, *Nat. Mater.,* 2013, **12**, 836-841.

7 Y. C. Hao, Y. Guo, L. W. Chen, M. Shu, X. Y. Wang, T. A. Bu, W. Y. Gao, N. Zhang, X. Su, X. Feng, J. W. Zhou, B. Wang, C. W. Hu, A. X. Yin, R. Si, Y. W. Zhang and C. H. Yan, *Nat. Catal.*, 2019, **2**, 448-456.

8 W. B. Qiu, Y. X. Luo, R. P. Liang, J. D. Qiu and X. H. Xia, *Chem. Commun.,* 2019, **55**, 7406-7409.

9 X. M. Yu, P. Han, Z. X. Wei, L. S. Huang, Z. X. Gu, S. J. Peng, J. M. Ma and G. F. Zheng, Joule, 2018, **2**, 1-13.

10 J. X. Zhao, B. Wang, Q. Zhou, H. B. Wang, X. H. Li, H. Y. Chen, Q. Wei, D. Wu, Y. L. Luo, J. M. You, F. Gong and X. P. Sun, *Chem. Commun.*, 2019, **55**, , 4997-5000.

11 G. S. Yu, H. R. Guo, W. H. Kong, T. Wang, Y. L. Luo, X. F. Shi, A. M. Asiri, T. S. Li and X. P. Sun, *J. Mater. Chem. A*, 2019, **7**, 19657-19661.

12 W. Y. Li, T. X. Wu, S. B. Zhang, Y. Y. Liu, C. J. Zhao, G. Q. Liu, G. Z. Wang, H. M. Zhang and H. J. Zhao, *Chem. Commun.,* 2018, **54**, 11188-11191.

13 P. F. Song, H. Wang, L. Kang, B. C. Ran, H. H. Song and R. M. Wang, *Chem. Commun.*, 2019, **55**, 687-690.

14 C. D. Lv, Y. M. Qian, C. S. Yan, Y. Ding, Y. Y. Liu, G. Chen and G. H. Yu, *Angew. Chem. Int. Ed.,* 2018, **57**, 10246-10250.

15 C. J. Zhao, S. B. Zhang, M. M. Han, X. Zhang, Y. Y. Liu, W. Y. Li, C. Chen, G. Z. Wang, H. M. Zhang and H. J. Zhao, *ACS Energy Lett.,* 2019, **4**, 377-383.

16 L. Xia, X. F. Wu, Y. Wang, Z. G. Niu, Q. Liu, T. S. Li, X. F. Shi, A. M. Asiri and X. P. Sun, *Small Methods*, 2019, **3**, 1800251.

17 Y. M. Liu, Y. Su, X. Quan, X. F. Fan, S. Chen, H. T. Yu, H. M. Zhao, Y. B. Zhang and J. J. Zhao, *ACS Catal.,* 2018, **8**, 1186-1191.